

Time-Resolved Imaging Reveals Transiently Chaotic Spin-Orbit-Torque-Driven Dynamics Under Controlled Conditions

L.-M. Kern,^{1,*} K. Litzius,^{2,*} V. Deinhart,^{3,4} M. Schneider,¹ C. Klose,¹ K. Gerlinger,¹ R. Battistelli,³ D. Engel,¹ C. M. Günther,⁵ M.-J. Huang,⁶ K. Höfflich,^{4,3} F. Büttner,^{2,3} S. Eisebitt,^{1,7} and B. Pfau¹

¹*Max Born Institute for Nonlinear Optics and Short Pulse Spectroscopy, 12489 Berlin, Germany*

²*Experimental Physics V, Center for Electronic Correlations and Magnetism,
University of Augsburg, 86159 Augsburg, Germany*

³*Helmholtz-Zentrum Berlin für Materialien und Energie, 14109 Berlin, Germany*

⁴*Ferdinand-Braun-Institut, Leibniz-Institut für Höchstfrequenztechnik, 12489 Berlin, Germany*

⁵*Technische Universität Berlin, Zentraleinrichtung Elektronenmikroskopie, 10623 Berlin, Germany*

⁶*Deutsches Elektronen-Synchrotron, 22607 Hamburg, Germany*

⁷*Technische Universität Berlin, Institut für Optik und Atomare Physik, 10623 Berlin, Germany*

Spin-orbit torques (SOTs) act as efficient drivers for nanoscale magnetic systems, such as magnetic tunnel junctions, nano-oscillators and racetrack geometries. In particular, in combination with materials exhibiting high Dzyaloshinskii–Moriya interaction, SOTs are considered to result in well-controlled deterministic magnetisation dynamics and are, therefore, used as robust drives to move and create magnetic skyrmions. In contrast to these expectations, we here find unpredictable, transiently chaotic dynamics induced by SOT at an artificial anisotropy-engineered defect in a magnetic racetrack. Based on these controlled conditions, we directly observe the nanoscale dynamics with holography-based, time-resolved x-ray imaging. In concert with micromagnetic simulations, we disclose a regime of violent picosecond fluctuations, including topological instabilities that, remarkably, result in deterministic final configurations. In addition, our images expose previously unseen skyrmion shedding and highlight the potential of transiently chaotic pathways for topological switching. Our approach offers new perspectives for the investigation and application of highly non-linear SOT dynamics in spintronics materials.

Spin-orbit torques (SOTs) belong to the most effective and efficient means to manipulate magnetisation via electric current [1, 2]. Advances in the conversion of electric into spin-polarised current have enhanced the SOT efficiency by leveraging interfacial effects between non-magnetic and magnetic layers [3], including the spin-Hall effect, the Rashba-Edelstein effect, magnons, and strain [1, 2]. SOTs find diverse applications in nanometre scale systems, such as switching magnetisation in magnetic tunnel junctions [4, 5], moving domain walls [6, 7], driving spin-wave emission and nano-oscillators [8, 9], and creating topologically non-trivial spin textures including magnetic skyrmions [10–12].

The high interest in SOTs arises from their potential for driving well-controlled deterministic dynamics in technological applications [13]. The ability to precisely predict the dynamics through micromagnetic simulations has contributed to a profound understanding of SOT dynamics and its anticipated technological relevance. As an example, SOT has emerged as optimal driver in racetracks of magnetic material with high Dzyaloshinskii–Moriya interaction (DMI), inducing continuous steady-state motion of chiral domain walls and skyrmions [7, 14–16]. Seamless and controlled dynamics have also been demonstrated in the context of SOT-driven skyrmion creation at anisotropy defects randomly distributed in the racetrack [11, 17].

Recently, localised anisotropy engineering via focused ion-beam irradiation has enhanced the control over this creation process via predefining the nanoscale creation site [18]. Using time-resolved imaging in this controlled environment, we here disclose that, surprisingly, the SOT can drive a system through a regime of unpredictable, chaotic dynamics characterised by magnetic fluctuations with topological instabilities. Remarkably, these dynamics still result in deterministic final configurations despite their transiently chaotic nature. The SOT-induced chaotic fluctuations also facilitate the emergence of hitherto unobserved dynamic magnetisation textures, similar to the predicted skyrmion shedding driven by spin transfer torque [19]. The direct observation of these dynamics already at moderate current densities points to a new transiently chaotic pathway for topological switching to create magnetic skyrmions.

Magnetic skyrmions, as the prototypical example for topologically non-trivial spin textures, can be stabilised in magnetic multilayers at room temperature with a chirality defined by the interfacial DMI [10–12]. These magnetic textures appear particle-like and, once fully controlled, could be used in information storage and spintronic applications [20, 21]. Direct observation of the SOT-driven magnetisation dynamics in skyrmion materials is challenging. To image the nano- and picosecond dynamics of spin textures on the sub-100 nanometre resolution level, x-ray pump-probe techniques in a repetitive, stroboscopic mode are required. Therefore, previous experiments investigating skyrmion dynamics had to rely on either confined geometries [22, 23], or highly

* These two authors contributed equally.

localised dynamics around a nanocontact [24] or a selected random defect [17, 25]. Here, we show that the introduction of the artificial anisotropy-engineered defect with nanometre precision establishes suitable conditions for pump-probe imaging at MHz repetition rates. We demonstrate a time-resolved x-ray imaging experiment to probe the response of the local magnetisation during and shortly after the SOT pulse. In concert with micromagnetic simulations, we find complex magnetisation dynamics that qualitatively and quantitatively change in dependence on the electric current density generating the SOT and the magnetic field applied.

In simulation and experiment, we study an asymmetrically stacked ferromagnetic multilayer consisting of 15 repeats of a Pt/Co₆₀Fe₂₅B₁₅/MgO trilayer with perpendicular magnetic anisotropy (PMA) and interfacial Dzyaloshinskii–Moriya interaction (DMI) (see Methods for more details), which today is one of the standard systems to study the SOT-driven creation and motion of magnetic skyrmions [11, 15, 16, 26, 27]. In the experiment, our magnetic material was structured into a racetrack geometry to allow for current-pulse injection into the device [11, 18], as shown in Fig. 1a and b. The key aspect of our device is creating a region of reduced anisotropy by local He⁺-ion irradiation of a circular region of 100 nm diameter positioned close to the centre of the magnetic racetrack. Moreover, enhanced SOT switching efficiencies have been observed in ion-irradiated regions [28, 29], allowing us to address these regions selectively with SOT [18]. This anisotropy-engineered region (from now on referred to as the “dot”) hence allows us to control the SOT-driven dynamics spatially.

To realise a pump-probe experiment as schematically depicted in Fig. 3b, we have to ensure that the dynamics is repeatable. As a minimum condition for repeatability, the initial state before the SOT pump and the relaxed state after the pump must be identical. Therefore, we performed micromagnetic modelling of the magnetisation dynamics triggered at a nanometre-sized dot of modified magnetic properties to predict suitable experimental parameters. The simulation area covers the full width and central part of the racetrack as shown in Fig. 1a. Our modelling is performed at zero-temperature and we keep the material parameters constant throughout our simulation runs (see Methods for details on the simulations).

In the simulation, two subsequent current pulses of 10 ns duration generate the SOT (Fig. 2a). First, the system is primed into a suitable state (e.g., a nucleation process). We consider this instance to initialise the pump-probe dynamics, resulting in reproducible dynamics within subsequent cycles. During the first 0.5 ns in the initialisation phase, the dynamics is spatially limited to the area of the dot, and we present snapshots cropped to the size of the dot in Fig. 2b. The dynamics always starts with a coherent spin canting in the whole dot. Above a nucleation threshold, a localised spin wave emerges, almost symmetrically propagates towards the centre of the dot, and, finally, leads to a completely reversed area at

the upper right edge of the dot. This reversed area finally relaxes to a magnetic bubble with either winding number $Q = 0$ or $Q = 1$ (skyrmion) in the dot. Below the threshold, the primed state is again uniformly magnetised.

The second pulse then excites this state, and the dynamics is further simulated until it becomes stationary again. The dynamics triggered by the second pulse actually simulates one experimental pump-probe cycle. In Fig. 2d, we map out different types of dynamics starting from a primed state and explore the influence of the current density, j_x , and the static applied field, H_z , which we use to control the dynamics in the experiment.

If the primed state is uniformly magnetised, the second pulse again triggers the spin canting, persisting during the entire pulse duration and then quickly returning to a homogeneous magnetisation (purple).

At low j_x and H_z , the magnetic bubble nucleated during the initialisation experiences only gentle perturbation from the SOT pulse, leading to breathing and a compression mainly along the direction of j_x . We denote this dynamics as the deformation dynamics. In contrast to this regime, the dynamics becomes much more violent inside the dot when increasing the current density. The response over a large region in our diagram involves strong magnetic fluctuations and instabilities on picosecond timescales (stripe-shaded region in the map).

At moderate applied fields (orange and light red), we additionally observe magnetic fluctuations extending outside the dot, which are highly mobile in the material. Complex periodically recurring states and transient instabilities of the magnetisation characterise these dynamics. They at first manifest as elongations originating from the dot (*stripe-out*, orange), which at even higher current density break off and form small, topological textures that move away from the dot. Similar magnetisation dynamics was already found in models with spin transfer torque, referred to as skyrmion *shedding* [19], here denoted in light red.

The magnetisation relaxes into two different states (Fig. 2e): either a homogeneous magnetisation (non-switched state) or a stable bubble at the position of the dot (switched state). Importantly, the system reliably returns to its initial switched or non-switched state over a wide range of experimental parameters, as required for pump-probe experiments, with only a few exceptions. These exceptions occur in particular at the boundaries of the phase diagram. The reproducibility of the initial and final states forms the basis for a pump-probe time-resolved imaging experiment, as discussed next.

The experiment was performed by directly imaging the SOT-driven dynamics and the transient magnetic configurations involved using time-resolved x-ray holography with sub-20 nm spatial resolution [30] (see Methods for details). We recorded data for a series of delays Δt between the 10 ns rectangular current pulse and the x-ray pulse with a duration of 100 ps, including image frames taken before, during, and after the current pulse arrives

in the racetrack. By tuning H_z and j_x , we explored the map of SOT-induced dynamics in our device and found evidence for the different types of dynamics predicted in our simulations, with two examples presented in Fig. 3. For each example, we show five representative snapshots from the time-resolved imaging alongside frames from simulation runs that qualitatively match our experimental results for equivalent applied fields and current densities (see Methods for details on comparing experimental and simulation parameters). The entire movies are provided in the Supplementary Material.

The first time series was recorded at an applied field close to saturation such that persistent nucleation of a skyrmion in the dot is not allowed [18]. Still, we observe a transient change of out-of-plane magnetisation inside the dot during and some nanoseconds after applying the SOT pulse (Fig. 3a). The magnetisation in the dot never entirely switches, though, and images taken before and several nanoseconds after the pulse appear homogeneously magnetised. This observation matches our simulation for this field regime, predicting only a transient coherent canting of spins in the dot. As the only difference, the experimentally detected dynamics is slower than the simulations predict, which we mainly attribute to the generic choice of the damping parameter in the simulations. This slowdown is consistently observed in all our experimentally recorded movies.

The type of dynamics dramatically changes when lowering the applied field to a regime where switching becomes possible (Fig. 3b). In this case, the first current pulse in the pump-probe experiment nucleates the magnetic texture in the dot, which is then present at the beginning of all following cycles. As a result, we generally detect a substantially increased contrast due to the switched magnetisation in the dot in line with the simulations. Most strikingly, we image SOT-driven deformation and elongation of the magnetisation texture evolving from the dot into the non-modified magnetic film, which finally results in the break-off and detachment of magnetic textures (Fig. 3b). More imaging examples of SOT-driven dynamics, including deformation and stripe-out, can be found in Extended Data Fig. 2.

Despite the notable agreement between our simulations and the experimental results in most aspects, we find one essential difference: During the SOT pulse, the magnetisation contrast in the experiment considerably reduces in the dot towards the end of the pulse—a behaviour we observe in the shedding regime but also when the dynamics is confined to the dot at higher applied field (Fig. 4a). This finding is particularly surprising as the skyrmion in the dot is clearly visible before and several nanoseconds after the current pulse. To understand this contrast reduction, we have to go back to our observation in the simulation that the magnetisation dynamics is characterised by instabilities and fluctuations when operating in a specific parameter space (stripe-shaded region in Fig. 2d). In this highly dynamic regime, magnetic textures recurrently appear in different shapes and then

quickly disappear, indicating chaotic behaviour.

Chaos is generally described by an extreme sensitivity of a system’s dynamic trajectories to its initial conditions. In our experiment, several parameters may contribute to a variation of these conditions, particularly thermal fluctuations, which are not included in the micromagnetic modelling. Therefore, we model the chaotic instability by performing two simulation runs with a slight variation (of 0.4%) of the current density generating the SOT while starting with an identical initial state for both runs. The results are presented in Fig. 4b, where we show snapshots of the magnetic state at equal times for the two runs. After the start of the SOT pulse, the magnetisation dynamics appear almost identical in both runs for the first 2 ns. However, after 4 ns, the transient magnetic textures become uncorrelated between the two runs. These practically unpredictable pathways of the dynamics also become apparent in seemingly random motion of the transient texture (see centre of mass in Fig. 4c) and random variation of its size (see magnetisation in Fig. 4d). These magnetisation fluctuations also involve frequent changes in winding number (Fig. 4e), producing transient skyrmionic textures. Altogether, our simulations confirm the chaotic nature of the dynamics, including topological transformations.

The image in the experiment is formed from an average of the millionfold repetition of the pump-probe cycle. The experimental conditions can differ in the individual cycles with respect to small shot-to-shot variations of current density or thermal spin fluctuations. In the chaotic regime, the dynamics is, therefore, expected to follow a different trajectory in each cycle. As a result, the increasing decorrelation of the magnetic states leads to a washing-out of the contrast. Therefore, we must not expect a one-to-one correspondence of the images from the experiment and modelling where the latter only describes the dynamics in a *single* selected cycle. However, aspects of the dynamics reproduced in every cycle still appear in our averaged x-ray images. As such, we can consistently detect a general shift of the “black” magnetic texture to the right in experiment (Fig. 4a) and simulation (Fig. 4c) as well as a general increase of positive (“white”) out-of-plane magnetisation (Fig. 4d). Despite the transient chaos, the final relaxed states simulated in both runs in Fig. 4b are very similar to each other and also to the initial state. Fully in line with this finding, we observe full magnetisation contrast in the experiment before the SOT pulse, and the contrast fully recovers after the SOT pulse.

The SOT-driven shedding process, which we here experimentally disclose (Fig. 3b), obeys the same dynamics: The stripe-out and break-off process is certainly governed and driven by chaotic fluctuations as witnessed by the simulations and the faint contrast of the transient magnetic features. However, it must clearly contain a “core” trajectory that consistently repeats in space and time to allow for our observation of a disconnecting magnetic texture. Notably, the chaotic contrast reduction is

experimentally not observed in regimes where the simulations predict canting or deformation dynamics. In these cases, the low SOT drive only gently perturbs the state without entering a fluctuation regime (Fig. 3a, Extended Data Fig. 2a).

Our findings are based on the introduction of the tailored defect (the 'dot'), which acts as the origin and return point for the SOT-induced magnetisation dynamics. It has deliberately modified magnetic properties, allowing us to investigate SOT-driven dynamics under controlled conditions in a real material in our simulations *and* in our experiment. We find complex, non-linear dynamics that strongly depend on the external parameters. At low SOT drive, we find canting, switching and breathing dynamics similar to what has been described earlier [17, 25]. Most importantly, our results show that chaotic fluctuations, which, thus far, were not anticipated for SOT-driven dynamics, now appear as an integral part of the dynamics in a large part of the parameter space investigated. As our zero-temperature simulations substantiate, the transient chaos is inherently included in the Landau-Lifshitz-Gilbert dynamics. In the experiment, the chaotic nature of the dynamics amplifies thermal fluctuations and pulse-to-pulse variations of the current density to unpredictable dynamic trajectories.

Remarkably, the transient chaos is already reached at moderate current densities, frequently used in experiments on skyrmions [11, 15, 17, 18, 24, 25, 31] and well below the destruction threshold of the device by Joule heating, even at MHz repetition rates (Extended Data Fig. 1d). Therefore, our results indicate that chaotic SOT-driven magnetisation dynamics play a much larger role in such experiments than considered so far. We have shown that the chaotic magnetic fluctuations involve topological transitions, which induce the formation of magnetic skyrmions inside and outside the dot. This new mechanism may also be required to form higher-order topological textures, such as skyrmionia recently found in a He⁺-ion processed material [18]. The transiently chaotic topological switching requires neither an assisting in-plane magnetic field nor the involvement of edge states [4].

The stripe-out of transient magnetic texture and the detachment (shedding) of skyrmions from an anisotropy defect have already been predicted by simulations based on spin transfer torque [19, 32]. We here directly prove the existence of such dynamics with time-resolved imaging for technologically relevant SOT drives. Similar physics has also been found for SOT-driven auto-oscillations at a nanocontact to an in-plane magnetized film [9]. These magnetic oscillations can form a localised magnetic droplet or spin-wave soliton at the nanocontact [33, 34] or even lead to the emission of spin waves into the magnetic film [8]. While these oscillations and spin-waves appear more coherent compared to our dynamics in an out-of-plane medium, our magnetic fluctuations, particularly the periodic shedding, can also be interpreted in terms of an emission of spin-wave-like dynamic textures.

In addition to these dynamic excitations, our material supports the emergence and stabilisation of static solitons such as the skyrmion. Therefore, we envision that devices like ours provide a highly desired platform for experiments and technological developments where highly dynamic textures interact with static skyrmions, domain walls or more complicated textures.

Highly non-linear dynamics and chaotic regimes are ubiquitous in nature [35], and their importance is increasingly recognised in modern descriptions of magnetisation dynamics [36–38]. Strikingly, spin-orbit torques can take a central role for triggering chaotic magnetisation dynamics beyond switching, such as enhanced spin-wave-like emission of dynamic textures,[8, 19, 39, 40] or chaos-mediated magnetisation reversal within fixed boundaries [36, 41]. While we usually aim for enhanced control over (magnetic) systems, especially with regard to technological devices, transient chaos can be exploited as a catalyst for topological switching, potentially connecting spin-wave and skyrmion dynamics. It may also find applications in chaos-based computing schemes [42] and probabilistic computing [43, 44]. Beyond their potential technological relevance, our results highlight the complex interplay between SOT drive and local magnetisation often present behind magnetic systems that are statically well understood and might spark further fundamental studies on chaotic regimes.

I. METHODS

A. Sample fabrication

Ferromagnetic multilayers with a nominal composition of Ta(3 nm)/Pt(4 nm)/[Pt(2.5 nm)/Co₆₀Fe₂₅B₁₅(0.7 nm)/MgO(1.4 nm)]₁₅/Pt(2 nm) were deposited on 500 nm thick Si₃N₄-membranes via argon-ion-assisted DC and RF magnetron sputtering. The magnetisation curve, as shown in Extended Data Fig. 1a, was recorded using magneto-optical Kerr microscopy. The domain width at remanence was determined via magnetic force microscopy to be ≈ 120 nm. In a magnetic film with the same nominal composition from a different fabrication run, we obtained a saturation magnetisation of $M_S = 1.28 \times 10^6$ A/m and an anisotropy constant $K_u = 1.55$ MJ/m³ via SQUID-magnetometry. To allow for current injection into the device, the magnetic film was structured into a magnetic racetrack geometry with a narrowed region of $3 \mu\text{m} \times 1 \mu\text{m}$, using a combination of UV lithography and focused Ga⁺-ion-beam milling (FEI Helios Nanolab 600) (see Extended Data Fig. 1b). In addition, employing UV lithography and electron-beam evaporation, gold contacts were deposited to the sides of the racetrack for wire bonding. For x-ray holography, the field of view is fixed to a circular region of 600 nm diameter defined by an otherwise x-ray opaque 1 μm thick gold mask layer on the back side of the SiN membrane. The monolithic integrated sample design [45] allows drift-free

operation [22]. Six pinholes of varying diameter between 20 and 110 nm were placed around the circular aperture to provide holographic reference beams. Next, the magnetic film was locally irradiated using a focused helium ion beam, similar to the work presented in Ref. [18]. Employing focused ion beams has the great advantage that preferred nucleation sites can be patterned with a high degree of control in terms of their shape and position as well as their anisotropy reduction. We prepared a circular area of 50 nm radius with an ion dose of 125 ions/nm², using the ZEISS Orion NanoFab He⁺-FIB and the FIB-o-mat software package [46]. Using a custom-developed sample aligning tool, FIB patterns are written with a placement accuracy of at least 200 nm by employing pre-recorded optical and scanning electron micrographs for sample navigation, avoiding any inadvertent ion irradiation. The irradiated areas are composed of filled circular shapes which are rasterised in concentric circles with a dwell time of 0.1 μ s and a pitch of 1 nm in x- and y-directions. For the patterning process, we used an acceleration voltage of 30 kV, a 20 μ m wide aperture and ion currents between 2.5 pA and 4 pA. Note here that we denote disks of 50 nm radius as “dots” throughout the main text.

The multilayer is entirely field-polarised at an applied field above $\mu_0 H_S = 110$ mT (see magnetisation curve in Extended Data Fig. 1). Lowering the applied field below $\mu_0 H_N = 78$ mT, the magnetisation in the He⁺-irradiated region switches spontaneously before the rest of the film eventually breaks into magnetic domains. Even above H_N , a single SOT pulse generated from electric current can still induce local magnetisation switching in this region, resulting in the formation of a skyrmion [18]. At $\mu_0 H_z = 78$ mT, we find the threshold current density to nucleate a skyrmion in the ion-irradiated region to be $j_0 \equiv j_x = 4.3 \times 10^{11}$ A/m². Throughout this work, we express the current density with respect to this reference current j_0 .

B. X-ray imaging

The magnetic imaging was carried out using resonant coherent x-ray imaging based on a holography in transmission geometry [45]. By tuning the x-ray wavelength to the Co L₃ resonance (at 1.59 nm), the x-ray magnetic circular dichroism provides contrast to the out-of-plane component of the magnetisation (m_z). We performed the experiment at the MAX-P04 holography endstation at beamline P04 of the synchrotron-radiation facility PETRA III, Hamburg. Combining the holographic image retrieval with refinements via phase-retrieval algorithms, we achieve almost diffraction-limited spatial resolution of 18 nm [30] and a temporal resolution limited by the x-ray pulse duration of 100 ps. During the imaging experiments, a variable out-of-plane magnetic field (H_z) was applied by a dipole electromagnet.

In order to perform a time-resolved pump-probe imag-

ing experiment, we synchronise a nanosecond-pulsed current excitation as the pump pulse to the soft-x-ray probe pulse at a repetition rate of 5.2 MHz, leading to a cycle period of 192 ns. Figure 1b schematically shows the experimental setup with the magnetic sample in the centre. A programmable pulse generator injects current pulses into the racetrack device. The arrival of the x-ray pulses at the sample (time-zero) is determined with an avalanche photo-diode (APD) mounted at the sample position. A back-illuminated CCD (2048 \times 2048 *pixels*) recorded the x-ray holograms with an accumulated exposure time of 9 s per delay step, which corresponds to an averaging over 4.7×10^7 pump-probe cycles in a single image.

As shown in Extended Data Fig. 1c, we apply rectangular, unipolar electric current pulses of 10 ns pulse duration that are known to produce skyrmions in comparable material stacks [11, 17, 18]. Prior to each time-resolved measurement, the sample was saturated at a magnetic field of $\mu_0 H_z = 300$ mT to erase all magnetic history. The static magnetic field applied (H_z) during the time-resolved imaging and the current density applied are indicated in the figure captions. Note that the images were intentionally recorded in a different order than the delay steps to avoid accumulating effects. Regularly taking a static image between the dynamic acquisition ensures that our sample stays intact and does not show any damage.

We additionally carried out finite-element simulations using a commercial-grade backward differentiation formula solver (COMSOL multiphysics package, COMSOL AB, Stockholm) to estimate the expected heat load on the sample induced by the pulsed current drive with a period of 192 ns. We combined the simulation of the electric potential with a subsequent heat transfer across the interfaces via an electromagnetic coupling, based on the time-dependent heat equation in a 2D model of the sample. Based on these finite-element simulations, we estimate the Joule heating of our samples during the pump-probe imaging for the current density j_0 (see Extended Data Fig. 1d). While the sample transiently reaches a temperature of 22 K above room temperature, we obtain a persistent residual heating of 9 K at our repetition rate. We do not expect such low residual heat to significantly alter our experimental observations.

C. Micromagnetic simulations

Micromagnetic simulations were performed with the MicroMagnum framework and custom extensions for the DMI and SOT. All parameters were scaled according to the effective medium approach [10] to obtain the dynamics of the 15-layer stack in a single simulated layer. The simulated area consisted of a cartesian grid with 1000 \times 1000 \times 1 cells in *xyz*-direction. Each cell has a lateral dimension of 1 nm \times 1 nm \times 78 nm, where the extension in *z*-direction corresponds to the thickness of

the entire experimental multilayer stack.

We used the following parameters: Gilbert damping $\alpha = 0.1$, saturation magnetisation $M_S = 1.28 \times 10^6$ A/m, exchange stiffness $A = 10$ pJ/m, DMI constant $D = -1.5$ mJ/m², and effective anisotropy field $H_K = 0.81$ T. The irradiated area of lower anisotropy was modelled by a circular area of 100 nm diameter in the center of the simulated square. Inside the area, the spin Hall angle $\theta_H = 0.15$ was used together with a reduced uniaxial anisotropy of $0.2K_u$. The outside was modelled with lower spin-torque efficiency of $\theta_H = 0.1$ and the full K_u .

The simulations encompassed exchange, anisotropy, stray field, DMI, and external field modules as well as a Slonczewski spin torque (SOT). The initial state was chosen to be empty and relaxed before applying a 10 ns current pulse. This was done to account for the experimental pump-probe method that chains together many cycles during a single recorded frame, effectively averaging them and thus putting very little weight on the first initial cycle. After the first current pulse, the system was relaxed to find the ground state before applying the second consecutive pulse of 10 ns. This second pulse constitutes an individual cycle of the pump-probe scheme. Finally, a third relaxation was performed to find the new relaxed state. Over a large range in our phase diagram in Fig. 2d, we find relaxed states mostly consistent with the initial state of the second SOT pulse. However, we observed two exceptions at the boundary between the regime of magnetic fluctuations and the canting regime. In these cases, the system relaxed to a non-switched state when initially started in a switched state. We avoided this region in the experiment.

Simulating an individual pump-probe cycle, we can investigate a single signature of the magnetic response to the current pump pulse, which complements our experimental findings. Note that introducing stochasticity in the simulations is not feasible to the extent our experiment can provide it. Increasing the number of simulated

pump-probe cycles is computationally very expensive and does not further advance our insights since it cannot account for slight temperature variations or magnetic inhomogeneities always present in the material.

We were required to use a factor of 2.5 higher current densities in the simulations to achieve the same response as in the experiment. We did not attempt to arbitrarily adjust the material parameters to further match the simulation with the experiment.

SUPPORTING INFORMATION

Extended Data includes Figures of the magnetisation curve of the magnetic film, the experimentally applied current pulse shape, the calculated current-induced temperature evolution, a time series for deformation dynamics, for stripe-out dynamics and chaotic fluctuations; Supplementary Material includes Movies of the magnetisation dynamics as discussed in the main paper Fig. 2 and Fig. 3.

ACKNOWLEDGEMENTS

The measurements presented in this work were carried out at PETRA III (DESY). We acknowledge DESY (Hamburg, Germany), a member of the Helmholtz Association HGF, for the provision of experimental facilities at PETRA III, beamline P04. The ion-beam patterning was performed in the Corelab Correlative Microscopy and Spectroscopy at HZB. Financial support from the Leibniz Association via Grant No. K162/2018 (OptiSPIN) and the Helmholtz Young Investigator Group Program is acknowledged. In addition, we would like to highlight the support from the EU COST Action CA 19140 (FIT4NANO).

-
- [1] F. Hellman, A. Hoffmann, Y. Tserkovnyak, G. S. Beach, E. E. Fullerton, C. Leighton, A. H. MacDonald, D. C. Ralph, D. A. Arena, H. A. Dürr, *et al.*, Interface-induced phenomena in magnetism, *Reviews of Modern Physics* **89**, 025006 (2017).
 - [2] Q. Shao, P. Li, L. Liu, H. Yang, S. Fukami, A. Razavi, H. Wu, K. Wang, F. Freimuth, Y. Mokrousov, *et al.*, Roadmap of spin-orbit torques, *IEEE Transactions on Magnetics* **57**, 1 (2021).
 - [3] J. Sinova, S. O. Valenzuela, J. Wunderlich, C. Back, and T. Jungwirth, Spin hall effects, *Reviews of Modern Physics* **87**, 1213 (2015).
 - [4] M. Baumgartner, K. Garello, J. Mendil, C. O. Avci, E. Grimaldi, C. Murer, J. Feng, M. Gabureac, C. Stamm, Y. Acremann, *et al.*, Spatially and time-resolved magnetization dynamics driven by spin-orbit torques, *Nature Nanotechnology* **12**, 980 (2017).
 - [5] V. Krizakova, M. Perumkunnil, S. Couet, P. Gambardella, and K. Garello, Spin-orbit torque switching of magnetic tunnel junctions for memory applications, *Journal of Magnetism and Magnetic Materials* **562**, 169692 (2022).
 - [6] L. Caretta, M. Mann, F. Büttner, K. Ueda, B. Pfau, C. M. Günther, P. Hession, A. Churikova, C. Klose, M. Schneider, *et al.*, Fast current-driven domain walls and small skyrmions in a compensated ferrimagnet, *Nature Nanotechnology* **13**, 1154 (2018).
 - [7] C. O. Avci, E. Rosenberg, L. Caretta, F. Büttner, M. Mann, C. Marcus, D. Bono, C. A. Ross, and G. S. Beach, Interface-driven chiral magnetism and current-driven domain walls in insulating magnetic garnets, *Nature Nanotechnology* **14**, 561 (2019).
 - [8] H. Fulara, M. Zahedinejad, R. Khymyn, A. Awad, S. Muralidhar, M. Dvornik, and J. Åkerman, Spin-orbit torque-driven propagating spin waves, *Science Advances*

- 5, eaax8467 (2019).
- [9] V. Demidov, S. Urazhdin, A. Anane, V. Cros, and S. Demokritov, Spin-orbit-torque magnonics, *Journal of Applied Physics* **127**, 170901 (2020).
- [10] S. Woo, K. Litzius, B. Krüger, M.-Y. Im, L. Caretta, K. Richter, M. Mann, A. Krone, R. M. Reeve, M. Weigand, *et al.*, Observation of room-temperature magnetic skyrmions and their current-driven dynamics in ultrathin metallic ferromagnets, *Nature Materials* **15**, 501 (2016).
- [11] F. Büttner, I. Lemesch, M. Schneider, B. Pfau, C. M. Günther, P. Helsing, J. Geilhufe, L. Caretta, D. Engel, B. Krüger, *et al.*, Field-free deterministic ultrafast creation of magnetic skyrmions by spin-orbit torques, *Nature Nanotechnology* **12**, 1040 (2017).
- [12] W. Legrand, D. Maccariello, N. Reyren, K. Garcia, C. Moutafis, C. Moreau-Luchaire, S. Collin, K. Bouzehouane, V. Cros, and A. Fert, Room-temperature current-induced generation and motion of sub-100 nm skyrmions, *Nano Letters* **17**, 2703 (2017).
- [13] S.-H. Yang, R. Naaman, Y. Paltiel, and S. S. P. Parkin, Chiral spintronics, *Nature Reviews Physics* **3**, 328 (2021).
- [14] A. Fert, V. Cros, and J. Sampaio, Skyrmions on the track, *Nature nanotechnology* **8**, 152 (2013).
- [15] K. Litzius, I. Lemesch, B. Krüger, P. Bassirian, L. Caretta, K. Richter, F. Büttner, K. Sato, O. A. Tretiakov, J. Förster, *et al.*, Skyrmion hall effect revealed by direct time-resolved x-ray microscopy, *Nature Physics* **13**, 170 (2017).
- [16] K. Litzius, J. Leliaert, P. Bassirian, D. Rodrigues, S. Kromin, I. Lemesch, J. Zazvorka, K.-J. Lee, J. Mulkers, N. Kerber, *et al.*, The role of temperature and drive current in skyrmion dynamics, *Nature Electronics* **3**, 30 (2020).
- [17] S. Woo, K. M. Song, X. Zhang, M. Ezawa, Y. Zhou, X. Liu, M. Weigand, S. Finizio, J. Raabe, M.-C. Park, *et al.*, Deterministic creation and deletion of a single magnetic skyrmion observed by direct time-resolved x-ray microscopy, *Nature Electronics* **1**, 288 (2018).
- [18] L.-M. Kern, B. Pfau, V. Deinhardt, M. Schneider, C. Klose, K. Gerlinger, S. Wittrock, D. Engel, I. Will, C. M. Günther, R. Liefferink, J. H. Mentink, S. Wintz, M. Weigand, M.-J. Huang, R. Battistelli, D. Metternich, F. Büttner, K. Höflich, and S. Eisebitt, Deterministic generation and guided motion of magnetic skyrmions by focused He⁺-ion irradiation, *Nano Letters* **22**, 4028 (2022).
- [19] K. Everschor-Sitte, M. Sitte, T. Valet, A. Abanov, and J. Sinova, Skyrmion production on demand by homogeneous dc currents, *New Journal of Physics* **19**, 092001 (2017).
- [20] C. Moreau-Luchaire, C. Moutafis, N. Reyren, J. Sampaio, C. Vaz, N. Van Horne, K. Bouzehouane, K. Garcia, C. Deranlot, P. Warnicke, *et al.*, Additive interfacial chiral interaction in multilayers for stabilization of small individual skyrmions at room temperature, *Nature Nanotechnology* **11**, 444 (2016).
- [21] A. Fert, N. Reyren, and V. Cros, Magnetic skyrmions: advances in physics and potential applications, *Nature Reviews Materials* **2**, 1 (2017).
- [22] F. Büttner, C. Moutafis, M. Schneider, B. Krüger, C. Günther, J. Geilhufe, C. v. K. Schmising, J. Mohanty, B. Pfau, S. Schaffert, *et al.*, Dynamics and inertia of skyrmionic spin structures, *Nature Physics* **11**, 225 (2015).
- [23] W. Jiang, P. Upadhyaya, W. Zhang, G. Yu, M. B. Jungfleisch, F. Y. Fradin, J. E. Pearson, Y. Tserkovnyak, K. L. Wang, O. Heinonen, *et al.*, Blowing magnetic skyrmion bubbles, *Science* **349**, 283 (2015).
- [24] S. Finizio, K. Zeissler, S. Wintz, S. Mayr, T. Weßels, A. J. Huxtable, G. Burnell, C. H. Marrows, and J. Raabe, Deterministic field-free skyrmion nucleation at a nanoengineered injector device, *Nano Letters* **19**, 7246 (2019).
- [25] S. Woo, K. M. Song, H.-S. Han, M.-S. Jung, M.-Y. Im, K.-S. Lee, K. S. Song, P. Fischer, J.-I. Hong, J. W. Choi, *et al.*, Spin-orbit torque-driven skyrmion dynamics revealed by time-resolved x-ray microscopy, *Nature Communications* **8**, 1 (2017).
- [26] K. Gerlinger, B. Pfau, F. Büttner, M. Schneider, L.-M. Kern, J. Fuchs, D. Engel, C. M. Günther, M. Huang, I. Lemesch, *et al.*, Application concepts for ultrafast laser-induced skyrmion creation and annihilation, *Applied Physics Letters* **118**, 192403 (2021).
- [27] I. Lemesch, K. Litzius, M. Böttcher, P. Bassirian, N. Kerber, D. Heinze, J. Zázvorka, F. Büttner, L. Caretta, M. Mann, *et al.*, Current-induced skyrmion generation through morphological thermal transitions in chiral ferromagnetic heterostructures, *Advanced Materials* **30**, 1805461 (2018).
- [28] J. Yun, Y. Zuo, J. Mao, M. Chang, S. Zhang, J. Liu, and L. Xi, Lowering critical current density for spin-orbit torque induced magnetization switching by ion irradiation, *Applied Physics Letters* **115**, 032404 (2019).
- [29] P. Dunne, C. Fowley, G. Hlawacek, J. Kurian, G. Atcheson, S. Colis, N. Teichert, B. Kundys, M. Venkatesan, J. Lindner, *et al.*, Helium ion microscopy for reduced spin orbit torque switching currents, *Nano Letters* **20**, 7036 (2020).
- [30] R. Battistelli, D. Metternich, M. Schneider, L.-M. Kern, K. Litzius, J. Fuchs, C. Klose, K. Gerlinger, K. Bagschik, C. Günther, W. Engel, C. Ropers, S. Eisebitt, B. Pfau, F. Büttner, and S. Zayko, Coherent x-ray magnetic imaging with 5 nm resolution, *Optica* (2023).
- [31] R. Juge, K. Bairagi, K. G. Rana, J. Vogel, M. Sall, D. Mailly, V. T. Pham, Q. Zhang, N. Sisodia, M. Förster, *et al.*, Helium ions put magnetic skyrmions on the track, *Nano Letters* **21**, 2989 (2021).
- [32] J. Masell, D. R. Rodrigues, B. F. McKeever, and K. Everschor-Sitte, Spin-transfer torque driven motion, deformation, and instabilities of magnetic skyrmions at high currents, *Physical Review B* **101**, 214428 (2020).
- [33] S. M. Mohseni, S. Sani, J. Persson, T. A. Nguyen, S. Chung, Y. Pogoryelov, P. Muduli, E. Iacocca, A. Eklund, R. Dumas, *et al.*, Spin torque-generated magnetic droplet solitons, *Science* **339**, 1295 (2013).
- [34] S. Bonetti, R. Kukreja, Z. Chen, F. Macià, J. M. Hernández, A. Eklund, D. Backes, J. Frisch, J. Katine, G. Malm, S. Urazhdin, A. D. Kent, J. Stöhr, H. Ohldag, and H. A. Dürr, Direct observation and imaging of a spin-wave soliton with p-like symmetry, *Nature Communications* **6**, 8889 (2015).
- [35] T. Tél and Y.-C. Lai, Chaotic transients in spatially extended systems, *Physics Reports* **460**, 245 (2008).
- [36] E. A. Montoya, S. Perna, Y.-J. Chen, J. A. Katine, M. d'Aquino, C. Serpico, and I. N. Krivorotov, Magnetization reversal driven by low dimensional chaos in a nanoscale ferromagnet, *Nature Communications* **10**, 543 (2019).

- [37] L. Shen, J. Xia, X. Zhang, M. Ezawa, O. A. Tretiakov, X. Liu, G. Zhao, and Y. Zhou, Current-induced dynamics and chaos of antiferromagnetic bimerons, *Physical Review Letters* **124**, 037202 (2020).
- [38] L. Liu, W. Chen, and Y. Zheng, Emergent mechanics of magnetic skyrmions deformed by defects, *Physical Review Letters* **131**, 246701 (2023).
- [39] S. Woo and G. S. Beach, Control of propagating spin-wave attenuation by the spin-hall effect, *Journal of Applied Physics* **122**, 093901 (2017).
- [40] A. V. Chumak, P. Kabos, M. Wu, C. Abert, C. Adelman, A. Adeyeye, J. Åkerman, F. G. Aliev, A. Anane, A. Awad, *et al.*, Advances in magnetics roadmap on spin-wave computing, *IEEE Transactions on Magnetics* **58**, 1 (2022).
- [41] J. Williame, A. Difini Accioly, D. Rontani, M. Sciamanna, and J.-V. Kim, Chaotic dynamics in a macrospin spin-torque nano-oscillator with delayed feedback, *Applied Physics Letters* **114**, 232405 (2019).
- [42] W. L. Ditto, K. Murali, and S. Sinha, Chaos computing: ideas and implementations, *Philosophical Transactions of the Royal Society A: Mathematical, Physical and Engineering Sciences* **366**, 653 (2008).
- [43] M. W. Daniels, A. Madhavan, P. Talatchian, A. Mizrahi, and M. D. Stiles, Energy-efficient stochastic computing with superparamagnetic tunnel junctions, *Physical Review Applied* **13**, 034016 (2020).
- [44] P. Talatchian, M. W. Daniels, A. Madhavan, M. R. Puffall, E. Jué, W. H. Rippard, J. J. McClelland, and M. D. Stiles, Mutual control of stochastic switching for two electrically coupled superparamagnetic tunnel junctions, *Physical Review B* **104**, 054427 (2021).
- [45] S. Eisebitt, J. Lüning, W. Schlotter, M. Lörger, O. Hellwig, W. Eberhardt, and J. Stöhr, Lensless imaging of magnetic nanostructures by x-ray spectro-holography, *Nature* **432**, 885 (2004).
- [46] V. Deinhart, L.-M. Kern, J. N. Kirchhof, S. Jürgensen, J. Sturm, E. Krauss, T. Feichtner, S. Kovalchuk, M. Schneider, D. Engel, *et al.*, The patterning toolbox fib-o-mat: Exploiting the full potential of focused helium ions for nanofabrication, *Beilstein Journal of Nanotechnology* **12**, 304 (2021).

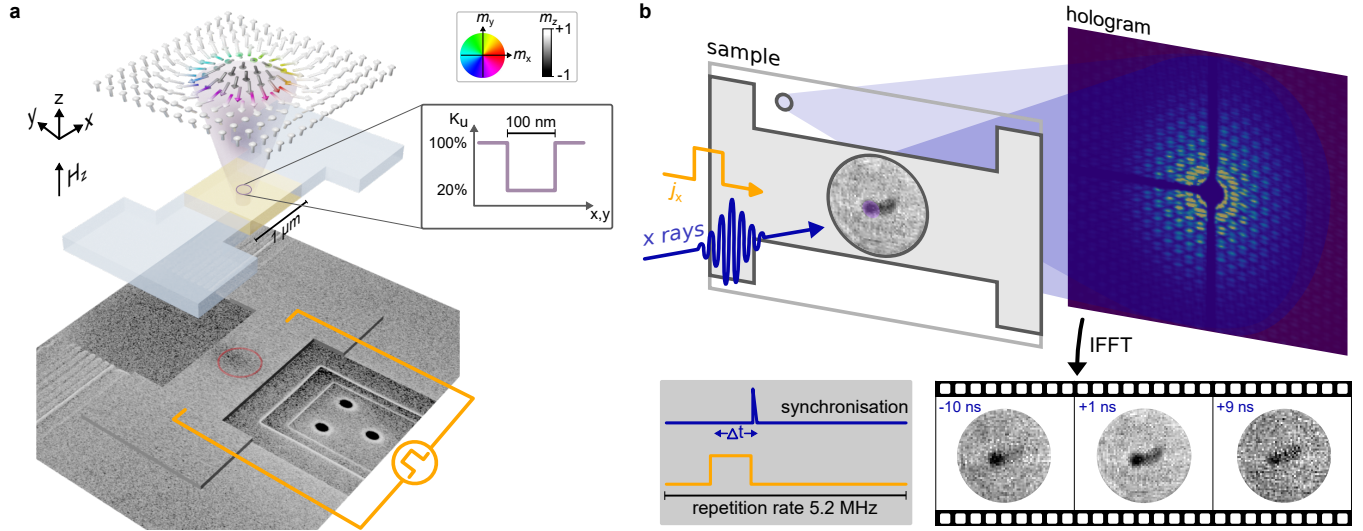


Fig. 1: Observing SOT-driven magnetisation dynamics in simulation and experiment. *a bottom:* Scanning electron microscopy (SEM) image of the magnetic racetrack device with the holographic field of view (red circle) and the electric connection for pulse injection indicated. *center:* Model of the device used for the simulation with the $1\ \mu\text{m}\times 1\ \mu\text{m}$ large area containing the anisotropy-engineered region in the centre. *top:* Illustration of the spin configuration in the dot after nucleating a skyrmion. *b* Schematic view of the pump-probe scheme for x-ray holography imaging of the current-induced SOT-driven magnetisation dynamics at an ion-irradiated region.

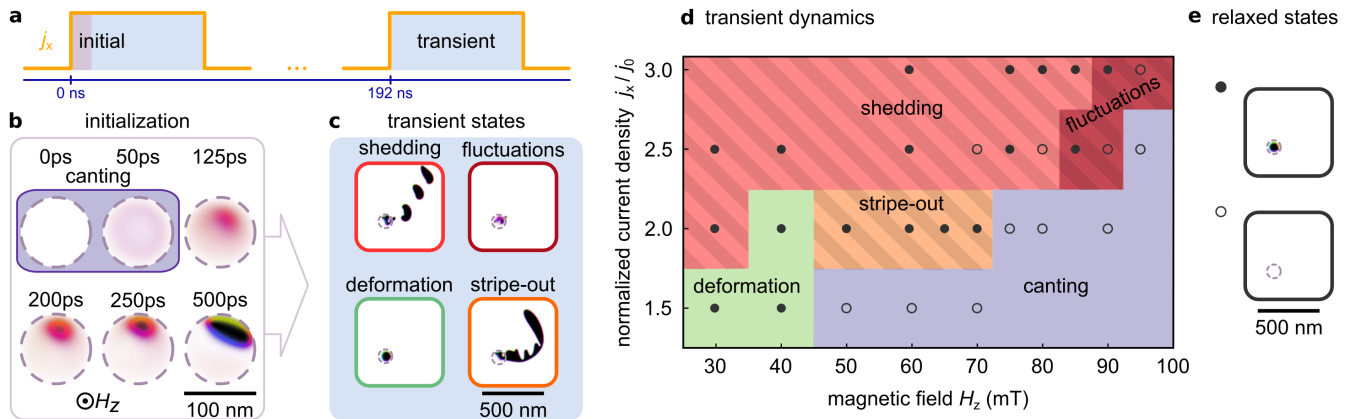


Fig. 2: Systematic modelling of magnetisation dynamics. *a* Two 10-ns current pulses are modeled. *b* The first pulse initialises a primed state with potential magnetisation switching. *c* The second pulse acts on the magnetisation state prepared, mimicking a cycle in the pump-probe scheme. All images are cropped to the same region of interest, with a dashed outline indicating the dot. *d* Phase diagram of corresponding dynamics in the parameter space of applied magnetic field and current density. Dots represent parameter values for which simulations were carried out. Fluctuations are observed in the stripe-shaded region. See Methods for details on j_0 . *e* The relaxed state is either (i) a bubble nucleated in the dot (filled circles in *d*), or (ii) a homogeneously magnetised state (open circles).

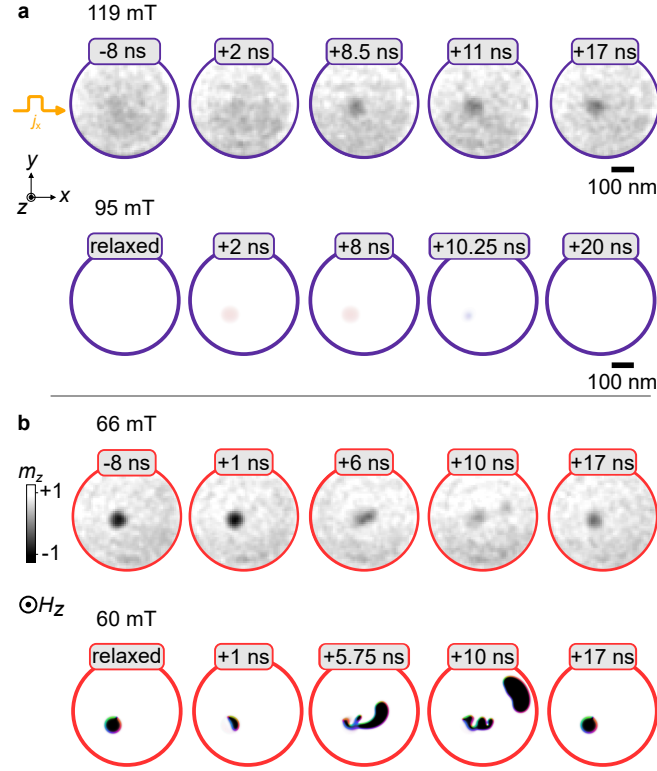


Fig. 3: Time-resolved imaging of magnetisation dynamics. The applied field used in the pump-probe experiment (top row in each panel) and simulation (bottom row) are indicated. The colour code corresponds to the dynamics introduced in Fig. 2. The field of view in the experiment is fixed to a circular region (diameter 600 nm) (see Methods), and simulation results were cropped to the same size. **a** Coherent spin canting inside the dot does not switch the magnetisation. **b** A detachment of transient topological textures from the switched dot marks the experimental evidence for skyrmion shedding. The entire movies are available in the Supplementary Material.

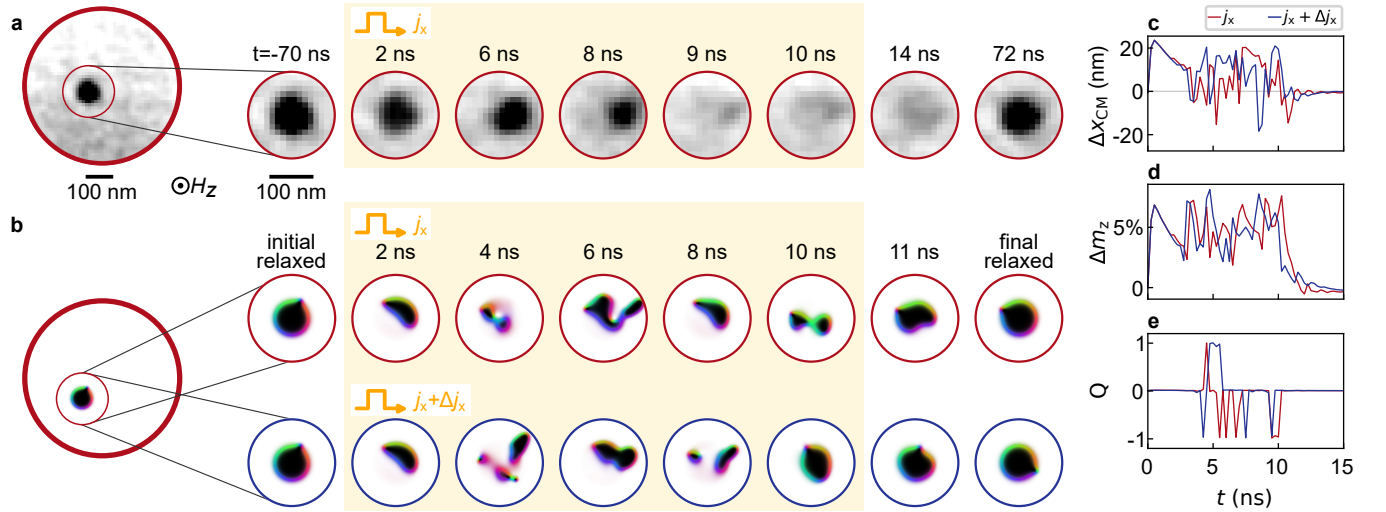
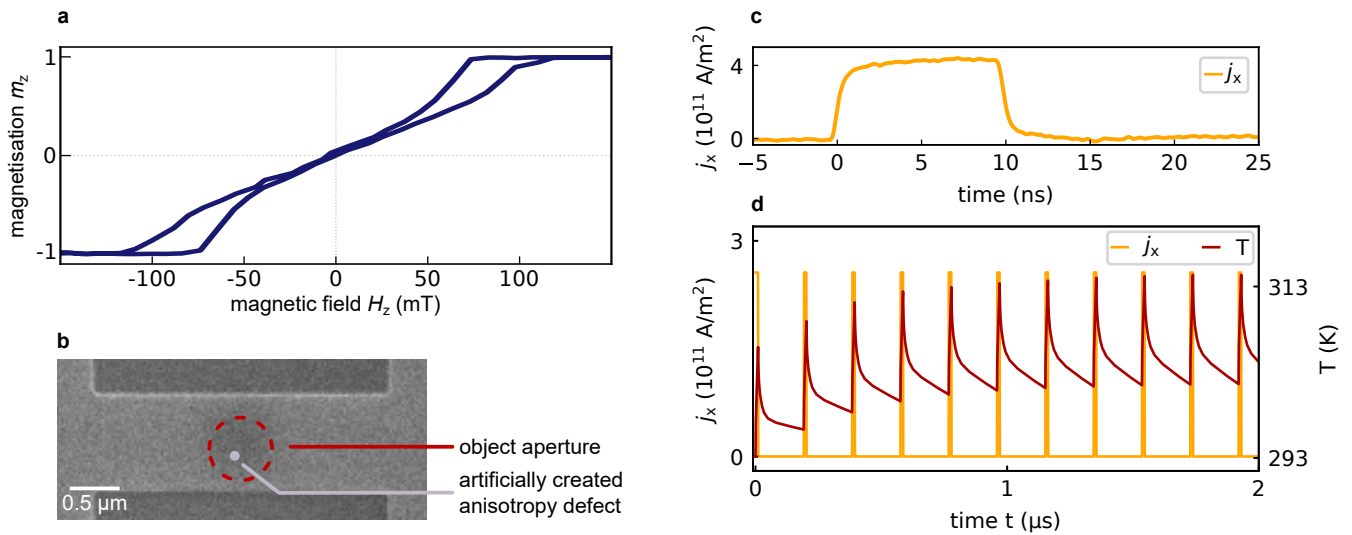
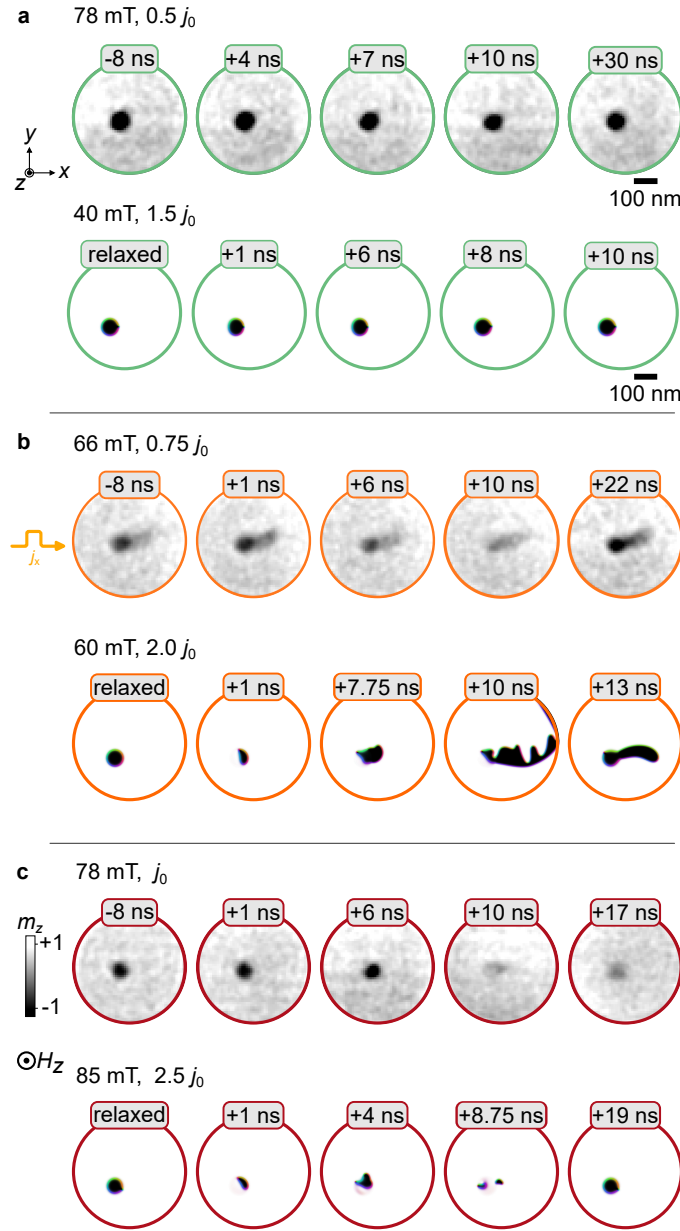


Fig. 4: Transiently chaotic SOT dynamics. **a** Time-resolved imaging results at $\mu_0 H_z = 78$ mT. The dynamics is restricted to the dot, and the averaged magnetisation contrast reduces towards the end of the pulse. **b** Two simulation runs with identical initial state but slightly different current density with difference $\Delta j_x / j_x = 0.4\%$. **c–e** Analysis of the dynamic textures in the two simulation runs relative to the initial state. **c** The centre of mass displacement along the x -direction, **d** the magnetisation difference (normalised to the 600 nm field of view), and **e** change in winding number.

EXTENDED DATA



Extended Data Fig. 1: Experimental Details. **a** Hysteresis curve of [Pt/CoFeB/MgO]-multilayer, recorded using magneto-optical Kerr microscopy. **b** Scanning electron microscopy image of the magnetic racetrack with an object aperture of 600 nm diameter (red) and an ion-irradiated anisotropy-engineered region of 100 nm diameter (purple). **c** Rectangular current pump pulses of 10 ns duration are injected into the device, synchronised to the bunch clock at a repetition rate of 5.2 MHz. The delay between current pump and x-ray probe beam is variable. **d** Simulations of the current-induced temperature evolution estimate a peak temperature of 22 K above room temperature and a static heating of 9 K of the magnetic film.



Extended Data Fig. 2: Time-resolved imaging of deformation, stripe-out and fluctuation dynamics.

The applied field and the current density used in the experiment (top row in each panel) and simulation (bottom row) are indicated. The colour code corresponds to the dynamics introduced in Fig. 2. The FOV in the experiment is fixed to a circular region (diameter 600 nm) (see main text and Methods for details). **a** Deformation. SOT from a low current density leaves the skyrmion almost unchanged during and after the current pulse, in line with the subtle deformation dynamics found in the simulations. Since the magnetisation contrast is not reduced, there is no experimental evidence for transient chaotic behaviour at this current density. Note that the experiment was performed at $j_x = 0.5j_0$, which is considerably below the single-pulse nucleation threshold j_0 . The initial state was therefore prepared with a single current pulse with $j_x = j_0$. **b** Stripe-out. The magnetisation stripes out and forms a tail of reduced contrast outside the dot. Towards the end of the pulse, also the contrast in the dot is clearly reduced. **c** Fluctuations. Full size of the images shown in Fig. 4. The transient chaotic dynamics are restricted to the area of the dot.